

## Vortex pinning in Josephson-junction arrays

M. S. Rzchowski, S. P. Benz, M. Tinkham, and C. J. Lobb\*

*Physics Department and Division of Applied Sciences, Harvard University, Cambridge, Massachusetts 02138*

(Received 1 March 1990)

Josephson-junction arrays provide a uniform lattice of vortex pinning sites. We investigate the effect of pinning on vortex motion in this model system through comparisons of numerical simulations with measurements on  $1000 \times 1000$  Nb-Cu-Nb proximity-effect Josephson-junction arrays. The resistive transition is broadened upon application of small magnetic fields near  $f=0$ , where  $f$  is the number of flux quanta per unit cell. We discuss this broadening in terms of thermally activated vortex motion. The resistive transition at  $f = \frac{1}{2}$  also broadens in the presence of small additional magnetic fields; we attribute this broadening to motion of field-induced defects in the ground-state vortex superlattice. Pinning barriers are found to be field independent for small deviations of the field from both  $f=0$  and  $\frac{1}{2}$ . We also discuss measurements suggesting defect motion near  $f = \frac{1}{3}$  and  $\frac{1}{4}$ . The implications of these results for flux-line lattice dissipation in other systems are discussed.

### I. INTRODUCTION

In zero magnetic field a two-dimensional array of coupled Josephson junctions is known to approach the zero-resistance state via a Kosterlitz-Thouless (KT) transition.<sup>1-3</sup> At low temperatures, the dominant thermal excitations are vortex-antivortex bound pairs that do not contribute substantially to the dissipation when driven by a small current. As the temperature is increased, the pairs begin to dissociate, giving rise to resistance. This has been theoretically described in the continuum limit,<sup>4</sup> and interpreted for the discrete case of Josephson-junction arrays by Lobb, Abraham, and Tinkham (LAT).<sup>5</sup> This Kosterlitz-Thouless behavior has been experimentally verified by a number of groups.<sup>6-8</sup> LAT have further shown that the interaction of vortices with the underlying lattice (energy scale  $\approx 0.2E_J$ ) is unimportant near the KT transition temperature [where  $k_B T \approx E_J(T)$ ].

In the limit of small applied magnetic field and temperatures well below the zero-field KT transition, interactions between the field-induced vortices are much smaller than those between the vortices and the Josephson-junction lattice. LAT have shown<sup>5</sup> that this interaction potential is due to a network of pinning sites, each at the center of a cell of the array. As will be shown in Sec. IV, the experimentally determined vortex pinning energy confirms the theoretical prediction (LAT) that it is much smaller than the energy scale of the KT transition. Hence vortices induced by an external magnetic field will be mobile in a range below the KT transition temperature, until thermal fluctuations become less than the pinning strength. These mobile vortices dominate the sample resistance in this temperature range, resulting in a dramatic broadening of the resistive transition upon application of small magnetic fields.

We will also argue that a similar picture is qualitatively valid near specific values of external magnetic field other than zero,<sup>9</sup> in particular in the case of "full frustration,"

or a field equivalent to  $\frac{1}{2}$  flux quanta per unit cell of the square array ( $f = \frac{1}{2}$ ). At zero temperature, every unit cell in the  $f = \frac{1}{2}$  ground state has a vorticity (determined from a circulating current) opposite in sign and equal in magnitude to its neighbors, forming a checkerboard pattern.<sup>10</sup> An increase in magnetic field equivalent to one additional flux quantum in the sample can induce a state where, qualitatively, a "minus" vorticity in one cell has changed to a "plus," as well as more complicated domain wall structures. The data of Sec. IV suggest that these "defects" in the  $f = \frac{1}{2}$  ground state are mobile at high temperatures in much the same way as a vortex in zero field.

This paper is organized as follows. Section II develops expressions for the pinning potential, mass, and viscous drag of the vortex, and the interaction of a vortex with a dc current. These are incorporated in a vortex equation of motion, from which the array current-voltage characteristic in the presence of thermal fluctuations is determined. Section III uses the relaxation method of LAT to calculate the critical current for single vortex motion in arrays of up to  $64 \times 64$  Josephson junctions with no resistive shunts. Critical currents are determined by the onset of instability in the static phase configurations. Section IV describes our experimental measurements of  $1000 \times 1000$  arrays of Nb-Cu-Nb proximity-effect junctions, determining the pinning barrier height and vortex density dependence through temperature-dependent resistance, current-voltage characteristic, and magnetoresistance measurements. Section V concludes the paper with a discussion of vortex pinning in more complex flux structures of the array, and the implications for flux-line lattice dissipation in other systems.

### II. VORTICES IN JOSEPHSON-JUNCTION ARRAYS

We consider a square lattice (lattice constant  $a$ ) where the horizontal and vertical bonds are Josephson junctions and the lattice sites are point islands of superconductor

(see Fig. 1). In this model, the Hamiltonian is the sum of individual junction energies and can be written

$$E_J \sum_{\langle ij \rangle} [1 - \cos(\phi_i - \phi_j - \psi_{ij})], \quad (1)$$

where  $\phi_i$  is the phase of the complex superconducting order parameter at site  $i$ , and

$$\psi_{ij} = (2e/\hbar c) \int_i^j \mathbf{A} \cdot d\mathbf{l}$$

is the integral of the vector potential along the junction between sites  $i$  and  $j$ .  $E_J$  is the Josephson energy  $\hbar i_c/2e$ , where  $i_c$  is the isolated junction critical current in the absence of fluctuations. The sum in Eq. (1) is over nearest neighbors only. In the limit in which current-induced magnetic fields are small compared with an externally imposed uniform field  $\mathbf{H}$  perpendicular to the array, the sum of  $\psi_{ij}$  around any unit cell must equal

$$2\pi H a^2 / \Phi_0 \equiv 2\pi f,$$

where  $f$  is the number of flux quanta enclosed by each unit cell.

The zero-temperature ground states of this system have been extensively studied,<sup>10-12</sup> and are described as arrangements of circulating currents similar to vortices in type-II superconductors. For values of  $f$  not close to an integer, these vortices are tightly packed and strongly interacting. For  $f$  of the form  $p/q$  with  $p$  and  $q$  small integers (i.e.,  $f = \frac{1}{3}, \frac{1}{4}, \frac{1}{2}, \frac{3}{4}$ ), the interacting vortex structure is also strongly coupled to the underlying junction lattice. In the limit of small  $f$ , on the other hand, the vortices act independently, and the only important interaction is with the underlying lattice.

It is in this limit that vortex motion, including the effects of vortex mass, viscosity, and pinning, can be most easily investigated. In the model system we have described, the *magnitude* of the superconducting order parameter is constant from site to site, and the state of the system can be completely described by specifying a phase

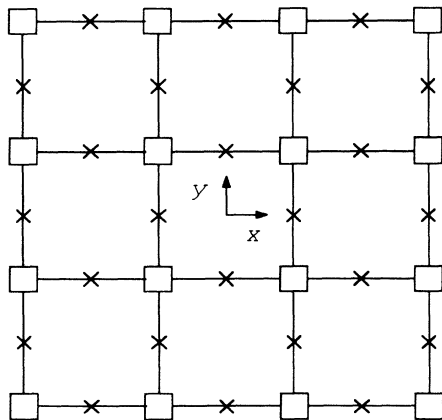


FIG. 1. Section of Josephson-junction array used in the numerical simulations. The boxes represent islands of superconductors, which have phases  $\phi_i$ , and the lines with crosses denote the Josephson junctions joining them.

at each island. If these are denoted by arrows centered at each site with the angle from the  $\hat{x}$  direction specifying the phase, a vortex is represented as a set of arrows pointing radially outward from the vortex "center." Figure 2 shows the result of a numerical simulation of a vortex, described in the next section.

In a similar numerical calculation, LAT showed that there are two positions corresponding to an extremum in the energy for such a vortex in a square lattice— that shown in Fig. 2, and an unstable state of higher energy where the vortex center is positioned *on* a junction rather than equidistant from the nearest four. Vortex motion out of one low-energy position and into an equivalent site one lattice constant away is thus prevented by a barrier, calculated<sup>5</sup> to be  $0.199E_J$  in the limit of large lattice size. An external current will exert a "Lorentz" force  $(1/c)j\Phi_0$  on the vortex, where  $j$  is the transport sheet current density in the array, and  $\Phi_0$  is the flux quantum. The interplay of this current, the pinning potential imposed by the Josephson-junction array, and thermal fluctuations determines the vortex motion and hence the resistance of the array.

This barrier height, along with the functional form of the vortex potential, will determine the critical current for vortex depinning. Using the "arctan" analytic approximation to the vortex phase configuration, we argue here that the vortex potential is very close to a pure sinusoid. In this approximation to a vortex,

$$\phi_i = \arctan[(y_i - y_0)/(x_i - x_0)],$$

the energy of the system for various vortex center posi-

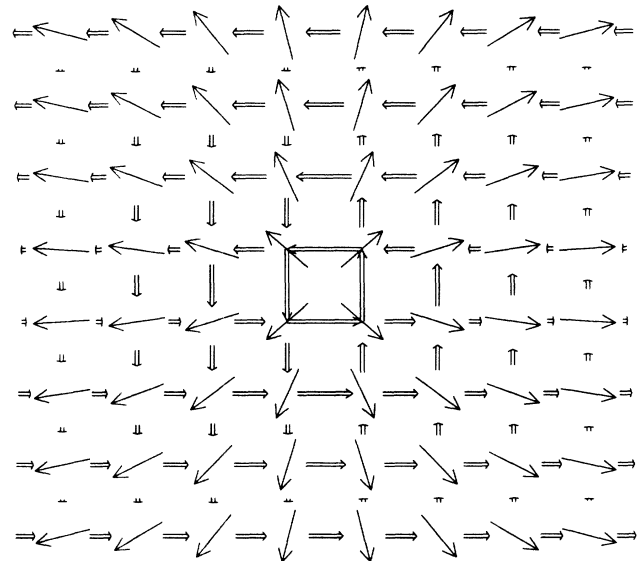


FIG. 2. Result of relaxation calculation for a vortex in an  $8 \times 8$  Josephson-junction array with zero applied field and no transport current. The angle of the single-line arrows from the  $x$  axis denotes the phase of the superconducting order parameter  $\phi_i$  at that node  $i$  (see Fig. 1). The length of a double-line arrow represents the magnitude of the current flowing through the junction on which it is centered. The distortion at the left and right edges of the array are caused by superconducting bus-bars (not shown) used to inject a transport current.

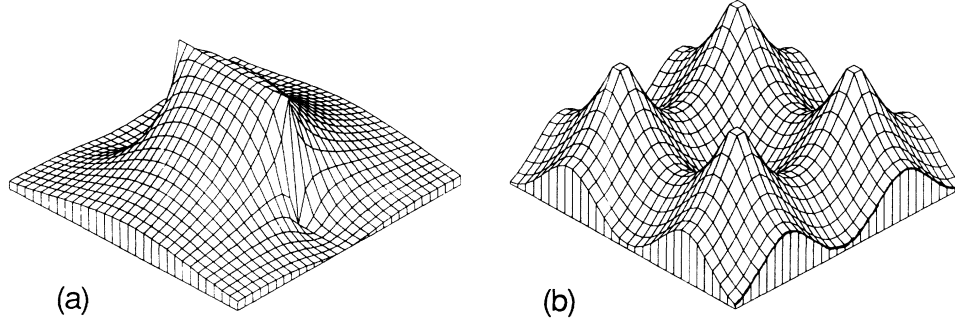


FIG. 3. (a) Contribution to the array energy from one Josephson junction as a function of vortex position  $(x, y)$ . The junction is at the center of the plot. (b) Central portion of an  $8 \times 8$  array, showing the net vortex potential obtained from summing the individual junction contributions shown in (a). The vortex is thermally activated from the low-energy position at the center of the graph.

tions  $(x_0, y_0)$  is easily computed as the sum of junction energies.<sup>13</sup> If, however, we consider the contribution of one junction to the system energy for various vortex positions around the junction, we can recast the problem as a particle moving in a square array of repulsive “molecules” that are centered on each junction, each with the interaction potential shown in Fig. 3(a), resulting in the total effective potential of Fig. 3(b). Because of this lattice structure, the total vortex potential is periodic with a fundamental wavelength of  $a$  in the  $\hat{x}$  and  $\hat{y}$  (see Fig. 1) directions, with higher harmonics restricted to reciprocal lattice vectors.<sup>14</sup> Because the single junction potential<sup>14</sup> has a characteristic length scale of  $a/2$  [see Fig. 3(a)], the Fourier content has decreased significantly at the second reciprocal lattice wave vector allowed by the array structure, and hence the fundamental Fourier component dominates the potential. In fact, a numerical Fourier transform shows that the second harmonic is more than a factor of 10 smaller than the fundamental.<sup>14</sup>

The zero-temperature critical current per junction for vortex motion,  $i_c^B$ , is reached when the transport current Lorentz force equals the maximum restoring force of the pinning potential. This gives  $i_c^B = eE_B/\hbar$  for a purely sinusoidal potential, where  $E_B$  is the barrier height. Using the numerical result<sup>5</sup>  $E_B = 0.199E_J$ , we find that  $i_c^B \approx 0.1i_c$ , where  $i_c$  is the single junction critical current. The correction to this critical current from the second harmonic contribution to the vortex potential is a factor of  $1 + 8(A_2/A_1)^2$ , equal to 1.08 for the arctan approximation, where  $A_2/A_1$  is the ratio of the second harmonic amplitude to the fundamental.

After depinning, the dynamics of a vortex are determined by its mass, and the viscosity of the surrounding medium.<sup>15</sup> A vortex moving with velocity  $v$  through a viscous medium dissipates energy at a rate  $\eta v^2$ , where  $\eta$  is the coefficient of viscous drag. Equating this to the sum of the power dissipated in each junction of the array, we have

$$\eta v^2 = \sum_{i,j} \frac{V_{ij}^2}{r_n}, \quad (2)$$

where  $v$  is the vortex velocity,  $V_{ij}$  is the voltage drop across the junction between islands  $i$  and  $j$ , and  $r_n$  is the

junction shunt resistance. (This viscous drag will in general be a function of vortex position in the unit cell—here we calculate an average drag coefficient, which will be most accurate for high vortex velocities.) Consider a vortex moving one cell starting in the configuration of Fig. 2. The junction that it crosses will have a change in phase difference of  $\pi$ , and by the Josephson relation will develop an average voltage drop of  $(\hbar/2e)(\pi/a)\bar{v}$ . This voltage creates normal currents in the array, which flow through a uniform lattice of equal junction shunt resistors  $r_n$ . This lattice of resistors presents an effective resistance<sup>16</sup> of  $r_n/2$ , and, apart from the difference between  $\bar{v}^2$  and  $v^2$  (which decreases as  $\bar{v}$  increases), an average drag coefficient can be written

$$\bar{\eta} \approx \left[ \frac{\hbar}{2e} \right]^2 \left[ \frac{2\pi}{a} \right]^2 \frac{1}{2r_n}. \quad (3)$$

This argument is qualitatively similar to that given by Bardeen and Stephen<sup>17</sup> for vortex dissipation in type-II superconductors, where half of the dissipation occurs in the normal core, and the rest in a region outside. The vortex mass can be calculated in a similar manner.<sup>18</sup>

Using the results for the vortex drag and lattice potential discussed above, we can write an equation of motion for a single vortex in a Josephson-junction array with transport current  $i$  per junction as

$$i_c^B \left[ \frac{i}{i_c^B} - \sin\theta \right] - \left[ \frac{\hbar}{2e} \right] \frac{1}{2r_n} \dot{\theta} + \tilde{i} = 0, \quad (4)$$

where  $i_c^B$  is the critical current per junction for *vortex motion* and  $\tilde{i}$  is a thermal noise current. Here we have specialized to the case of overdamped junctions of negligible capacitance (as in the proximity-effect arrays described in Sec. III and IV), and made the substitution  $\theta \equiv 2\pi x/a$ . Equation (4) is identical to the equation of motion for the phase difference across a *single* overdamped Josephson junction of parallel resistance  $2r_n$ , bias current  $i$ , critical current  $i_c^B$ , and thermal noise current  $\tilde{i}$ . The average voltage at finite temperature for this case has been computed by Ambegaokar and Halperin (AH).<sup>19</sup> Remembering that the phase difference across the *array* changes by  $2\pi$  when the vortex moves

across its width, and that the critical current  $I_c^B$  of a square array scales with the number of junctions  $N$  on a side, we can write the AH current-voltage characteristic for the array containing a single vortex as

$$\langle V \rangle = \frac{2r_n}{N^2} I_c^B \frac{2}{\omega} (1 - e^{-\pi\omega\alpha}) T_1^{-1}, \quad (5)$$

where

$$\omega = \frac{E_B}{k_B T}, \quad \alpha = \frac{i}{i_c^B}, \quad T_1 = \int_0^{2\pi} e^{-\omega\alpha u} I_0 \left[ \omega \sin \frac{u}{2} \right] du$$

and  $I_0$  is the modified Bessel function of zero order. For low currents and temperatures, this agrees with the thermally activated flux flow approximation<sup>20</sup> applied to the case of a single vortex in a periodic potential. For currents well above the vortex depinning current  $i_c^B$ , but still below the single junction critical current  $i_c$ , the array is Ohmic with resistance  $2r_n/N^2$ . In the intermediate regime, Eq. (5) must be integrated numerically. Equation (5) describes the resistance of the array resulting from the motion of one vortex. In the limit of low vortex densities (where vortices can be considered to be noninteracting), the voltage across the array will be proportional to the number of vortices, whether they are field induced or the result of thermal fluctuations. In the case of field-induced vortices in an  $M \times N$  array, where the current flow is along the  $M$  direction,  $\langle V \rangle / I$  consists of a prefactor  $2r_n f(M/N)$  (the flux-flow resistance) multiplying a function that approaches 1 as the current or temperature increases. At sufficiently high temperature or large current, Eq. (5) will break down as thermal fluctuations become large enough to nucleate additional vortices and vortex-antivortex pairs, and the array resistance rises to that of the normal state independent of the applied magnetic field.

### III. NUMERICAL SIMULATIONS OF VORTEX MOTION

We have simulated the static phase configurations for a junction array containing one vortex in the presence of a transport current, with and without an applied magnetic field. The junctions are modeled as Josephson junctions with no resistive shunt, so that any dynamic evolution of the phases will be incorrect in detail. We calculate the zero-temperature critical current as the highest current for which a stable phase configuration exists. The geometry of the sample studied is shown as an inset to Fig. 4. The  $N$  junctions on either end of the  $N \times N$  array are each tied to a superconducting busbar of constant gauge-invariant phase, where the transport current is introduced. We do not implement periodic boundary conditions at any of the edges.

The simulations are done with the Hamiltonian of Eq. (1) using a relaxation technique.<sup>5</sup> Minimizing this energy with respect to variations of the phases leads to a set of constraints on each  $\phi_i$  equivalent to current conservation at every superconducting island,

$$\sum_j \sin(\phi_i - \phi_j - \psi_{ij}) = 0, \quad (6a)$$

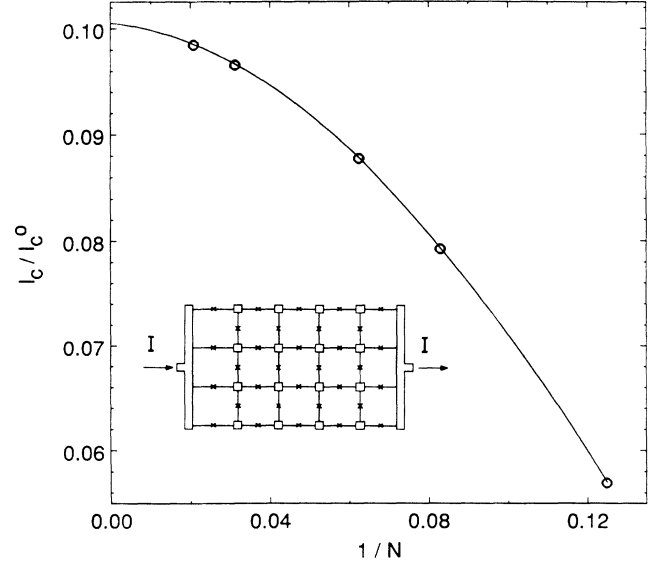


FIG. 4. Simulated critical current per junction of a Josephson-junction array containing one vortex, normalized to the single junction critical current, as a function of lattice size  $N$  in zero magnetic field. The infinite lattice extrapolation (solid line) is consistent with the  $0.1i_c$  result discussed in the text. The inset shows the position of the current busbars.

where the sum is over nearest neighbors. This can be solved for  $\phi_i$  in terms of the nearest-neighbor phases and the vector potential, resulting in  $N^2$  coupled nonlinear equations for the  $\phi_i$ . Each of these can be solved iteratively as

$$\tan(\phi_i^{(n+1)}) = \frac{\sum \sin(\phi_j^{(n)} + \psi_{ij})}{\sum \cos(\phi_j^{(n)} + \psi_{ij})}.$$

A transport current is introduced by specifying a net current into the left busbar and out of the right busbar. The equation determining the left busbar phase is then

$$\sum_j \sin(\phi_L - \phi_j - \psi_{Lj}) = I, \quad (6b)$$

where  $\phi_L$  is the left busbar phase,  $I$  is the injected transport current (see inset to Fig. 4), and the sum now runs over the  $N$  islands that are Josephson-coupled to the busbar. Equation (6b) can be solved iteratively for the left busbar phase, which is then included in the relaxation process. This method of current injection allows the current to flow nonuniformly at the edges if this would result in a reduction of the total energy. We introduce a vortex by using the arctan approximation as an initial condition. Although the dynamics of the simulation are not correct in detail, the vortex is stable for small currents, and is observed to hop from cell to cell once the critical current is exceeded. It ultimately leaves the array, which then relaxes into a phase configuration corresponding to uniform current flow.

In zero magnetic field, the critical current determined from the onset of instability of the phase configuration is shown in Fig. 4. The extrapolated critical current in the limit of large lattice size is  $(0.105 \pm 0.005)i_c$ , consistent

with a value of  $0.1i_c$  calculated from a barrier height  $0.199E_J$  and a purely sinusoidal vortex potential. The small magnitude of the possible discrepancy indicates a contribution from the second harmonic of the potential approximately ten times less than that for the arctan approximation of Sec. II.

These zero-field simulations describe a thermally excited vortex in the array. We have also calculated the vortex depinning current in a magnetic field producing  $\Phi_0$  of flux through the array, which results in one field-induced vortex. The simulations were done in the same manner as those in zero field, and the symmetric gauge

$$\mathbf{A} = \frac{1}{2}B(x\hat{y} - y\hat{x})$$

with origin at the zero-current vortex center was used so that the arctan representation approximates the actual phase configuration closely enough to be used as an initial condition for the relaxation process. The data in zero and nonzero applied field converge in the limit of large sample size, where the contribution of the vector potential is unimportant.

We have also considered the motion of a single extra vortex in an applied field of  $f = \frac{1}{2}$ . We generate a single vortex in the sample at  $f = \frac{1}{2}$  by relaxing from an initial condition of the  $f = \frac{1}{2}$  ground state with each phase perturbed by

$$\delta\phi_i = \arctan[(y_i - y_0)/(x_i - x_0)] .$$

As in the  $f = 0$  relaxation, we do not impose periodic boundary conditions at any of the edges. For large lattices, we find the energy relative to the relaxed  $f = \frac{1}{2}$  ground state with finite boundaries  $\approx E_J[0.96 + 2.15 \ln(N/2)]$  for an  $N \times N$  array. The size dependence is consistent with a perturbation calculation<sup>21</sup> giving

$$E \approx (\pi E_J / \sqrt{2}) \ln(N/2) .$$

In the  $f = \frac{1}{2}$  ground state, an equivalent site for the vortex center is not the adjacent site, but one two cells away. The adjacent cell is a high-energy position for the vortex center, in analogy with the high-energy position between two islands in the case of  $f = 0$  (see Sec. II). For this high-energy position in the  $f = \frac{1}{2}$  case, the cell containing the vortex has two units of positive vorticity. We have calculated the energy difference between the high- and low-energy positions for a vortex in the  $f = \frac{1}{2}$  ground state, finding that it extrapolates to  $\Delta E = (1.28 \pm 0.05)E_J$  in the limit of large lattices (arrays of up to  $64 \times 64$  junctions were simulated). A critical current associated with this barrier could not be confirmed in our static simulations, due to domain nucleation around the vortex and at the edges of the sample as the current was increased, but with the assumption of a sinusoidal vortex potential of period  $2a$ , the depinning current would be

$$i_c^B / i_c = \frac{1}{4} E_B / E_J \approx 0.32 .$$

This is close to the  $f = \frac{1}{2}$  ground-state critical current<sup>10,11</sup> of  $0.414i_c$ , in contrast to the case of  $f = 0$ , where the vortex depinning current was found to be ten times smaller

than the ground-state critical current.

This picture of vortex motion suggests that a vortex in the  $f = \frac{1}{2}$  state has approximately six times higher pinning energy than in the  $f = 0$  state. Different patterns of single vortex motion, for instance, a diagonal path to avoid occupied lattice cells, may result in a lower pinning barrier. However, it is likely that other processes of flux motion, associated with defects in domain walls, will occur in the  $f = \frac{1}{2}$  state. Domain walls in the  $f = \frac{1}{2}$  state divide regions where the pattern of alternating plus and minus cell vorticities (discussed in Sec. I) on either side of the wall are out of register with one another by one lattice constant. Teitel<sup>22</sup> has calculated ground states near  $f = \frac{1}{2}$  where domain walls with multiple defects proliferate. Halsey<sup>23</sup> has discussed domain walls with corners of  $\pm \frac{1}{4}$  local vorticities. A ‘‘jog’’ in a domain wall resulting in a one lattice constant offset in the wall but no change in direction has a vorticity of  $\pm \frac{1}{2}$ . This jog will propagate along the wall under the influence of transport current, producing dissipation in the same manner as the vortices discussed previously. Our preliminary simulations suggest that the barrier for this process may be lower than that for the simple vortex motion discussed above.

#### IV. EXPERIMENTAL PROCEDURE AND RESULTS

In this section we describe experimental measurements of  $1000 \times 1000$  Nb-Cu-Nb proximity-effect Josephson-junction arrays, concentrating on the effects of an external magnetic field on the resistive transition. The dominant effect is a dramatic broadening of the transition, shown in Fig. 5 for various applied magnetic fields, which

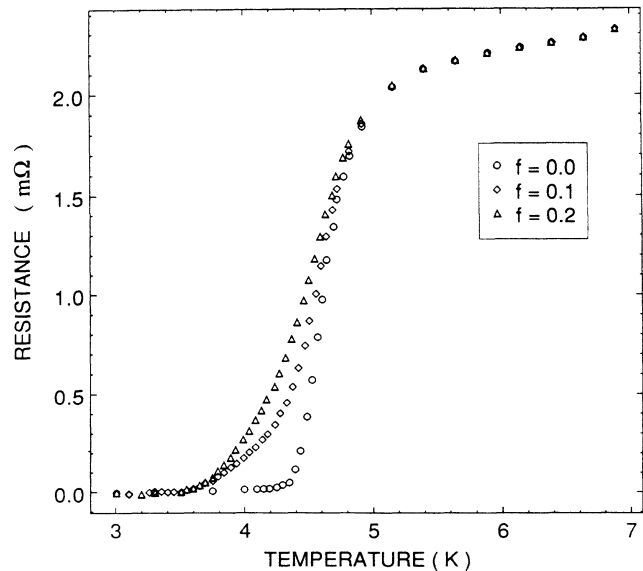


FIG. 5. Resistive transition of  $1000 \times 1000$  Nb-Cu-Nb Josephson-junction array in magnetic fields corresponding to  $f = 0, 0.1$ , and  $0.2$ . An ac excitation current of 30 nA per junction was used for the measurement. The great broadening of the transition in small magnetic fields is explainable by thermally activated motion of pinned vortices.

we investigate in terms of the vortex pinning model developed in the preceding sections. We extract pinning barrier heights and flux-flow resistances from the data, as well as verify the applicability of the single vortex model through magnetoresistance and current-voltage characteristic measurements. These measurements are made in small fields ( $f \ll 1$ ) as well as in fields near full frustration [ $(f - \frac{1}{2}) \ll 1$ ]. Thermally activated resistive transitions have been noted previously in junction arrays,<sup>8,24</sup> and attributed to isolated vortex motion. We take this approach in the limit of very small fields, and discuss thermally activated motion of defects in the  $f = \frac{1}{2}$  ground state for fields near full frustration.

The samples consist of 0.2- $\mu\text{m}$ -thick cross-shaped Nb islands on top of a continuous 0.3- $\mu\text{m}$ -thick copper underlayer.<sup>25,26</sup> The copper is thermally evaporated onto an Ar ion cleaned sapphire substrate. The sample is then moved to a dc magnetron sputtering system, where the copper surface is Ar ion etched immediately before Nb deposition. A subsequent liftoff of underlying photoresist defines the edges of the array. The remaining processing step involves photolithographic patterning of the superconducting islands, followed by SF<sub>6</sub> reactive ion etching. The resulting array has a distance between Nb island centers of 10  $\mu\text{m}$  and junctions 4  $\mu\text{m}$  wide with a separation of 2  $\mu\text{m}$ .

The niobium transition temperature for all of our samples is in the range 8.8–9.0 K, and the KT transition to the low-resistance state varies from 3.5 to 4.5 K. The normal state resistance of the arrays is approximately 2 m $\Omega$ . Because these are proximity-effect junctions, the coupling energy  $E_J$  is a strong function of temperature,<sup>27</sup> determined experimentally from measurements of the array critical current through the relation

$$E_J(T) = \hbar i_c(T) / 2e .$$

We determine the critical current as that current which corresponds to the maximum differential resistance of the array.<sup>28</sup> These currents are typically a factor of 100 times larger than our voltage threshold “critical currents” (where effects of vortex-antivortex pair breaking are important), hence we believe that our measurements of the array critical currents are indicative of isolated junction characteristics, and not seriously distorted by cooperative effects between junctions.

The four-terminal measurements described here were made with a PAR 124A lock-in amplifier with a rms ac excitation current of 30 nA per junction at 28 Hz. With a 1:100 coupling transformer at the input and a time constant of 30 s, noise levels of 300 pV are obtained. The junction arrays could be cooled to 1.4 K in a pumped <sup>4</sup>He system inside a double mu-metal shield. The temperature was controllable to well above the Nb transition, and stable to  $\pm 1$  mK. A solenoid was used to null any remaining ambient magnetic fields, and to apply fields to the sample.

Figure 6 shows the low-field resistive transitions on a logarithmic scale as a function of  $E_J(T)/k_B T$  ( $\equiv \gamma$ ) for two samples with zero-field critical temperatures differing by 0.7 K.<sup>29</sup> We have analyzed the data of Fig. 6 to extract a value for the pinning barrier and the prefactor of

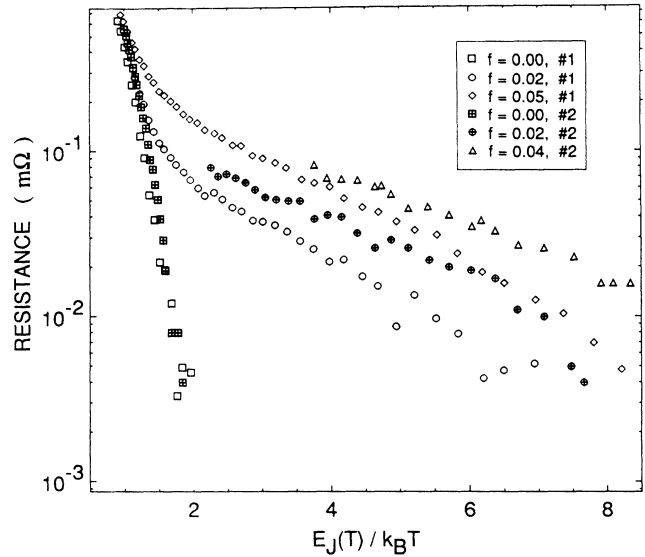


FIG. 6. Resistive transition of junction arrays near  $f=0$  as a function of the normalized coupling strength  $E_J(T)/k_B T$ , showing the thermally activated nature of the transition in a magnetic field. Samples 1 and 2 have zero-field transition temperatures of 4.3 K and 3.6 K, respectively.

the thermally activated behavior. Because the ratio of the measuring current to the vortex depinning critical current ( $i_c^B$ ) changes as the junction coupling energy changes, and we are not always in the small-current limit, the barrier and prefactor must be extracted from the data through a fit to Eq. (5) rather than a direct slope measurement. The measuring current for both of the samples was fixed at 30 nA per junction. By fitting the data, we find  $E_B \approx (0.34 \pm 0.03)E_J$ , and a prefactor of  $(1.7 \pm 0.1)R_n f$ . The prefactor is in agreement with our prediction of  $2R_n f$ , but the barrier is a factor of 1.7 larger than our result  $E_B = 0.2E_J$  of Sec. II. The finite resistance evident in the zero-field data of Fig. 6 at values of  $\gamma$  larger than the predicted KT transition ( $\gamma \approx 1.05$ ) is somewhat greater than the Monte Carlo results of Mon and Teitel,<sup>30</sup> which give voltages corresponding to  $\approx 5\%$  of the normal-state sample resistance at  $\gamma = 1.25$  for a single junction transport current  $i = 0.2i_c$ , but it may still be attributable to current-induced depairing. [Our measuring current per junction at  $\gamma = 1.25$  is approximately  $0.17i_c(T)$ .]

It has been suggested<sup>31</sup> that the magnetic-field broadening of the resistive transition in a system showing KT behavior can be explained by an increase of the dielectric constant due to screening by additional free vortices injected by the external magnetic field. This stimulates vortex depairing near  $T_c$ , effectively broadening the transition. This may in fact play a role very close to the KT transition in our samples, but these free vortices, unless pinned, would contribute a flux flow resistance  $2R_n f$  (see Sec. III) even at low temperatures. The decrease of our sample resistance at low temperatures to values less than the flux-flow resistance indicates that pinning effects are dominant in this regime.<sup>32</sup>

We have carried out similar measurements of the resistive transition in small increments of field around  $f = \frac{1}{2}$ . The data of Fig. 7 show the resistive transition at  $f = \frac{1}{2}$  to be broader than that at  $f = 0$ , with a characteristic  $\gamma_c$  roughly twice that of the  $f = 0$  transition, in agreement with numerical simulations.<sup>9</sup> On application of small increments of field, the transition broadens further, developing a thermally activated “tail” similar to that seen near  $f = 0$ . Although, for the case of  $f = \frac{1}{2}$ , we have not justified the use of the vortex motion model developed in Sec. II, a fit done as for the  $f = 0$  case yields a barrier of  $(0.44 \pm 0.02)E_J$  and a prefactor of  $(3.7 \pm 0.2)r_n f$ . This barrier is 1.3 times larger than the experimentally determined  $f = 0$  pinning barrier, suggesting that the type of vortex motion investigated in Sec. II for  $f = \frac{1}{2}$  [for which a barrier of  $6E_B(f = 0)$  is predicted] may not be correct in detail. The tail in the  $f = \frac{1}{2}$  transition beginning at  $\gamma \approx 4$  is possibly an effect of field inhomogeneity inducing a small “free” vortex population.

We have further characterized vortex pinning behavior at  $f = 0$  by analysis of the array current-voltage characteristic. Figure 8 shows the 2.50-K dynamic resistance ( $dV/dI$ ) as a function of dc bias current for fields of  $f = 0.00$  and  $f = 0.04$ . Since both the thermally activated vortex motion and the thermal fluctuations of the phase difference across a single junction can be described in the formalism of AH, we interpret the large peak in  $dV/dI$  at  $\approx 2$  mA as the single junction critical current, and the smaller, thermally broadened “peak” below 1 mA as the current associated with reducing the barrier for vortex motion to zero. With the assumption of a purely sinusoidal vortex potential, the critical current  $i_c^B$  associated with the thermal activation barrier  $E_B$  is given

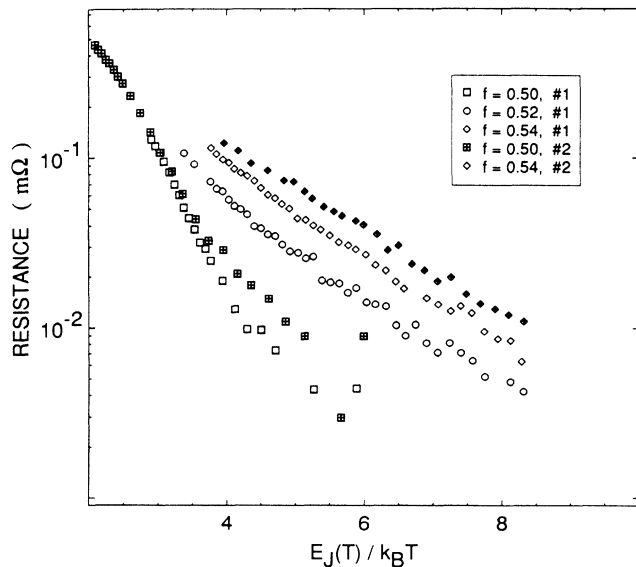


FIG. 7. Resistive transition of the junction arrays of Fig. 6 near  $f = \frac{1}{2}$  as a function of the normalized coupling strength  $E_J(T)/k_B T$  showing thermally activated behavior of mobile defects in the  $f = \frac{1}{2}$  ground state (see text). Samples 1 and 2 have zero-field transition temperatures of 4.3 K and 3.6 K, respectively.

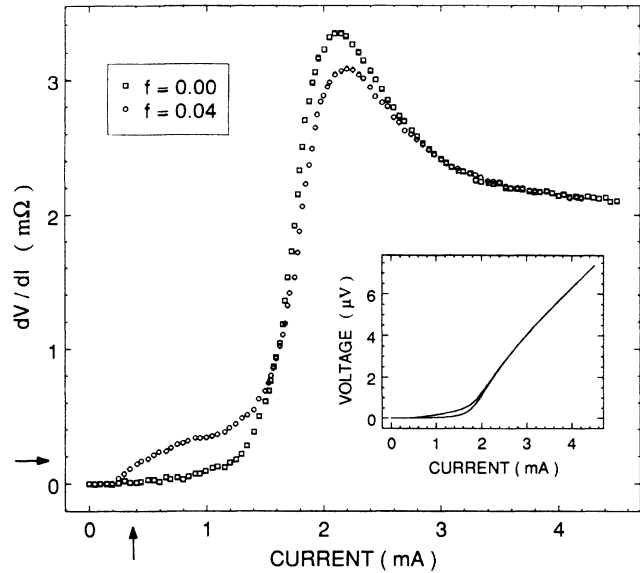


FIG. 8. Dynamic resistance ( $dV/dI$ ) at 2.5 K vs current for  $f = 0.00$  and  $0.04$ . The peak at  $I = 2.1$  mA indicates the isolated junction critical current. Application of a magnetic field introduces structure at low current indicating depinning of field-induced vortices. The depinning critical current and flux-flow resistivity calculated from the data of Fig. 6 are indicated by arrows. The inset shows  $V$  vs  $I$  obtained by direct integration of the data.

by  $i_c^B/i_c = \frac{1}{2}E_B/E_J$  (see Sec. II). At currents high enough that the vortex is completely depinned, but low enough that dissipation associated with the underlying  $f = 0$  background state is negligible,  $V/I$  (or  $dV/dI$ ) should approach the flux flow resistance from the prefactor of the thermal activation data (see Sec. II). Arrows on the axes indicate the values for depinning current and flux flow resistance obtained in this manner from the low-current thermally activated resistance of Fig. 7. The predicted depinning current is in general agreement with the data, but the low-current dissipation in the  $f = 0$  state (possibly due to stray fields induced by transport currents in the leads) increases the value of the resistance plateau above the flux flow resistance. A simple subtraction of the two curves at low current improves the agreement, which suggest the consistency of an activated vortex motion picture of the dissipation. At  $f = \frac{1}{2} + \delta f$ , a similar experimental verification is not possible. The distinctive shoulder of the  $f = 0.04$   $dV/dI$  data is not apparent, possibly because of domain structures nucleated by large transport currents.

Our interpretation is based on the picture of a single vortex interacting with the lattice structure of the junction array. There are, however, many vortices in the sample, even at the relatively small fields investigated here. Experimentally, we can establish the unimportance of vortex-vortex interactions by verifying that the resistance is directly proportional to the number of vortices in the sample. The data of Figs. 6 and 7 are consistent with this proportionality, but a more direct verification can be obtained through a measurement of the magnetoresistance. Figure 9 shows the resistance versus magnetic

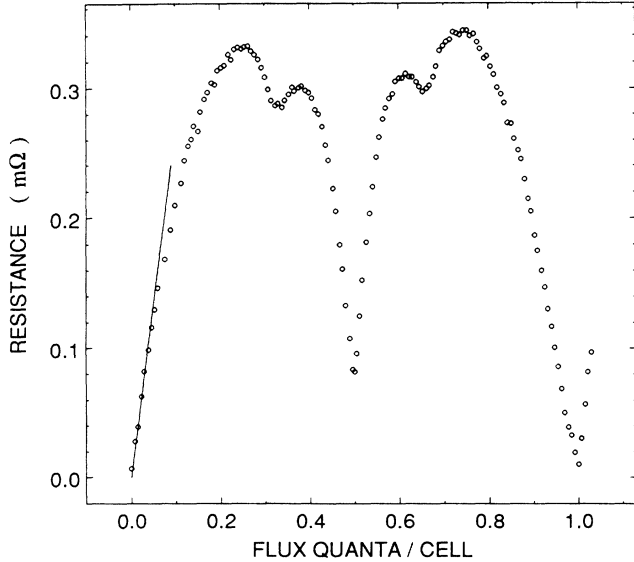


FIG. 9. Magnetoresistance of Josephson-junction array at  $T = 3.2$  K. The structure at  $f = \frac{1}{3}$ ,  $\frac{2}{3}$ , and  $\frac{1}{2}$  reflect pinning of the entire vortex superlattice when it is commensurate with the underlying Josephson-junction lattice. Note the linear increase in resistance with magnetic field near  $f = 0$ , 1, and  $\frac{1}{2}$ . The straight line is a linear fit to the data up to  $f = 0.05$ .

field at 3.2 K for a sample with zero-field  $T_c \approx 3.5$  K and normal-state resistance  $\approx 2.1$  m $\Omega$ . The minima at  $f = \frac{1}{2}$  and at  $f = \frac{1}{3}, \frac{2}{3}$  indicate the commensuration of the field-induced vortex superlattice with the array lattice structure, and the resulting large *superlattice* pinning strength. Measurements concentrating on the regions near  $f = 0$  and  $f = 0.5$  show a linearity of the magnetoresistance to  $\delta f \approx 0.05$ . The deviation of the magnetoresistance below its small  $\delta f$  linear behavior beyond this value indicates a reduction of thermal activation due to vortex-vortex interactions. We interpret this as an increase in the single vortex pinning barrier due to a collective restoring force from other (pinned) vortices.

## V. DISCUSSION AND CONCLUSIONS

### A. Magnetic fields of $f = 0$ and $f = \frac{1}{2}$

We have studied vortex pinning in large arrays of Josephson junctions through measurements of the resistive transition and current-voltage characteristics in magnetic fields. We have made these measurements in a magnetic-field regime where the absence of significant vortex-vortex interactions has been experimentally verified by the linear behavior of the magnetoresistance, and hence the applicability of the model of an isolated particle in a potential well developed in Sec. II. These measurements show that the broadening of the resistive transition in a magnetic field is due to noninteracting vortex motion near  $f = 0$ , and to superlattice defect motion near  $f = \frac{1}{2}$ . Fitting the finite-temperature solution [Eq. (5)] of this equation of motion to the data, we have deter-

mined a pinning strength of  $(0.34 \pm 0.03)E_J$  in the  $f = 0$  limit.

This value is not in agreement with our numerical simulations (Sec. III), which find the vortex depinning current in a perfect lattice at zero temperature to be  $\approx 0.1i_c$ , corresponding to a barrier  $\approx 0.2E_J$ . We have not completely validated, however, our determination of the critical current of a single junction from that measured in the array. A correction in this parameter would be directly reflected in the  $E_J/k_B T$  axis of Figs. 6 and 7. Nonuniform current flow in the array, for instance, would result in an artificially low value of the critical current, thereby increasing the ratio of the measured thermal activation barrier to this inferred  $i_c$ , and tending to account for the discrepancy between our experimental and theoretical values for the pinning barrier height. Correcting the critical current measurement because of such a nonuniform current flow, however, would move the value of  $E_J/k_B T$  associated with the Kosterlitz-Thouless transition to a value too high to easily justify. A second possibility is a nonuniformity of the array junction strengths, due either to a spacing variation, or a variation in the interface quality. This would result in a distribution of vortex pinning energies, and a dependence of the effective pinning barrier on temperature as strongly pinned vortices were frozen out. Our measurement of the critical currents of two isolated junctions on opposite sides of the same substrate indicate a variation of  $i_c$  on the order of 10%. A variation of this magnitude, if random from junction to junction, could add *extrinsic* pinning comparable to that required to explain the discrepancy between a predicted intrinsic barrier of  $0.2E_J$  and the measured value of  $(0.34 \pm 0.03)E_J$ . If  $i_c$  varied with a uniform gradient across the sample, however, the effect would be negligible.

A comparison which is independent of a simple scale correction to the critical current measurement is the ratio of energy barriers at different magnetic fields. We showed experimentally in Sec. IV that

$$E_B(f = \frac{1}{2})/E_B(f = 0) \approx 1.3$$

In Sec. III we theoretically analyzed one type of “vortex” motion in the  $f = \frac{1}{2}$  state, finding an effective barrier of  $\approx 6E_B(f = 0)$ . This disparity suggests that a more complex dynamical evolution, as discussed in Sec. III, is responsible for the dissipative motion. The experimentally determined  $(0.44 \pm 0.02)E_J$  defect pinning energy at  $f = \frac{1}{2}$  is, however, large enough in comparison with the characteristic energy of the  $f = \frac{1}{2}$  transition (an average slope from Fig. 7 is  $2.2E_J/k_B T$ ) that pinning of thermal excitations in the  $f = \frac{1}{2}$  state is likely to play a strong role in the resistive transition.

### B. Intermediate values of magnetic field

The magnetoresistance is linear in  $\delta f$  near  $f = 0$  and  $f = \frac{1}{2}$ , indicating the unimportance of vortex-vortex interactions near  $f = 0$ , and of defect-defect interactions near  $f = \frac{1}{2}$ . At slightly larger values of  $\delta f$ , we find that the magnetoresistance becomes sublinear, and prelimi-

nary measurements of the resistive transition indicate a magnetic-field dependence of the barrier height and prefactor, which we attribute to vortex-vortex interactions. As  $\delta f$  increases, these interactions will favor a superlattice structure of the field-induced vortices consistent with the underlying structure of the array.<sup>10</sup> Thermal fluctuations stronger than these interactions will minimize any such tendencies.

Teitel and Jayaprakash<sup>10</sup> propose that, for low enough temperature, the magnetoresistance is linear in  $\delta f$  about all values of field  $f_0$  for which the vortex superlattice is commensurate with the junction array, due to activated defect motion similar to that we have discussed in the case of  $f = \frac{1}{2}$ . The superlattice is in fact commensurate for all  $f = m/n$ , where  $m$  and  $n$  are integers, but in some of these states thermal fluctuations are larger than energies of "defects" and defect pinning energies, thus minimizing any effects of the commensuration. The magnetoresistance of Fig. 9 shows a sharp minimum when the induced vortex superlattice is commensurate with the underlying junction lattice of  $f = \frac{1}{2}$ , and  $f = \frac{1}{3}, \frac{2}{3}$ . In order to reliably measure isolated defect motion, the temperature must be low enough that the density of thermally activated defects is below the level where defect-defect interactions become important. This is evidenced by a linear behavior of the magnetoresistance around the commensurate field. The rounded minima at  $f = \frac{1}{3}$  and  $\frac{2}{3}$  in the magnetoresistance of Fig. 9 suggest a substantial defect population at this temperature. At low temperatures, pinning barriers become strong enough that low-current magnetoresistance measurements are not possible with our voltage sensitivity. These barriers, however, can be decreased by application of a large transport current.<sup>33</sup> With an applied current of  $0.55I_c$  ( $f=0$ ), we find the linearity of the magnetoresistance near  $f = \frac{1}{3}, \frac{2}{3}$  to be well developed at 2 K, with strong indications of similar behavior at  $f = \frac{1}{4}$  and  $\frac{1}{6}$ . Thermally activated behavior near these magnetic fields would be determined by the defect pinning energies and viscosities in a manner similar

to the data presented for  $f=0$  and  $\frac{1}{2}$ . Our measurement accuracy prevented a determination of activation barriers for defects in array ground states other than  $f=0$  and  $\frac{1}{2}$ .

The fields at which we have made measurements, however, provide examples of two extremes of flux flow dissipation: isolated vortex motion in the case of fields near  $f=0$ , and evolution of a distorted vortex superlattice near  $f = \frac{1}{2}$ . The experimentally measured barrier of only  $(0.44 \pm 0.02)E_J$  near  $f = \frac{1}{2}$  indicates a mechanism of thermal activation different than the motion of the vortexlike defect discussed in Sec. II, where the theoretical barrier was found to be  $1.3E_J$ . Such processes may include the growth of closed domains under the influence of a transport current,<sup>30</sup> or the motion of "kinks" in an extended domain wall.<sup>23</sup>

In contrast to the case of  $f=0$ , the barrier for motion of these defects is determined primarily by the structure of the vortex superlattice, and only indirectly by the discrete nature of the junction array. The pattern of the perfect vortex superlattice is enforced by the arrangement of junctions in the array, but the motion of defects in the superlattice is governed by the interaction of vortices in the superlattice. In this sense, the strongly interacting vortex states of the array provide a model system for studying thermally activated flux lattice distortions in more complicated systems,<sup>34</sup> and the straightforward nature of the junction array makes a direct theoretical analysis practical.

#### ACKNOWLEDGMENTS

We wish to thank M. G. Forrester for designing the array masks, H. Rogalla for invaluable advice and guidance in sample fabrication, and M. Cohn and G. O. Zimmerman for their assistance in the numerical simulations. This research was supported in part by National Science Foundation Grant Nos. DMR-86-14003 and DMR-89-12927, Office of Naval Research Grant No. N00014-89-J-1565, and Joint Services Electronics Program Grant No. N00014-89-J-1023.

\*Present address: Department of Physics, University of Maryland, College Park, MD 20742.

<sup>1</sup>J. M. Kosterlitz and D. J. Thouless, *J. Phys. C* **6**, 1181 (1973).

<sup>2</sup>J. M. Kosterlitz, *J. Phys. C* **7**, 1046 (1974).

<sup>3</sup>M. R. Beasley, J. E. Mooij, and T. P. Orlando, *Phys. Rev. Lett.* **42**, 1165 (1979); S. Doniach and B. A. Huberman, *ibid.* **42**, 1169 (1979); a review of the KT transition in thin films and Josephson junction arrays can be found in J. E. Mooij, in *NATO Advanced Study Institute on Advances in Superconductivity*, edited by B. Deaver and J. Ruvalds (Plenum, New York, 1983), p. 433.

<sup>4</sup>B. I. Halperin and David R. Nelson, *J. Low Temp. Phys.* **36**, 599 (1979).

<sup>5</sup>C. J. Lobb, David W. Abraham, and M. Tinkham, *Phys. Rev. B* **27**, 150 (1983).

<sup>6</sup>D. J. Resnick, J. C. Garland, J. T. Boyd, S. Shoemaker, and R. S. Newrock, *Phys. Rev. Lett.* **47**, 1542 (1981); David W. Abra-

ham, C. J. Lobb, M. Tinkham, and T. M. Klapwijk, *Phys. Rev. B* **26**, 5268 (1982); R. F. Voss and R. A. Webb, *ibid.* **25**, 3446 (1982).

<sup>7</sup>B. K. Brown and J. C. Garland, *Phys. Rev. B* **33**, 7827 (1986).

<sup>8</sup>J. P. Carini, *Phys. Rev. B* **38**, 63 (1988).

<sup>9</sup>S. Teitel and C. Jayaprakash, *Phys. Rev. B* **27**, 598 (1983).

<sup>10</sup>S. Teitel and C. Jayaprakash, *Phys. Rev. Lett.* **51**, 1999 (1983).

<sup>11</sup>Thomas C. Halsey, *Phys. Rev. B* **31**, 5728 (1985).

<sup>12</sup>W. Y. Shih and D. Stroud, *Phys. Rev. B* **28**, 6775 (1983).

<sup>13</sup>By characterizing the response of the Josephson junction array in terms of vortex motion, we are already making the approximation that the system can be completely described by the vortex center, rather than the phases at each of the  $N^2$  islands. Larkin *et al.* have shown that the arctan approximation overestimates the pinning barrier (see Ref. 15), but it will serve to illustrate our arguments for the form of the vortex potential.

<sup>14</sup>These Fourier components for an infinite lattice are given by

$$A_{k_x, k_y} = e^{i\pi\eta_x} F(n_x, n_y) + e^{i\pi\eta_y} F(n_y, n_x),$$

$$k_{x,y} = \frac{2\pi n_{x,y}}{a}$$

where

$$F(n_x, n_y) = \int_{-\infty}^{\infty} du dv f(u, v) e^{-2\pi i n_x u} e^{-2\pi i n_y v}$$

and

$$f(u, v) = 1 - \frac{u^2 + v^2 - (1/2)^2}{\{[u^2 + v^2 + (1/2)^2] - v^2\}^{1/2}}$$

is the single junction vortex potential energy shown in Fig. 3.

<sup>15</sup>The vortex mass in a junction array has been calculated in a different approximation by A. I. Larkin, Yu. N. Ovchinnikov, and A. Schmid, *Physica B* **152**, 266 (1988).

<sup>16</sup>S. Kirkpatrick, *Rev. Mod. Phys.* **45**, 574 (1973).

<sup>17</sup>J. Bardeen and M. J. Stephen, *Phys. Rev.* **140**, A1197 (1965).

<sup>18</sup>A similar argument, starting from

$$\frac{1}{2} M v^2 = \sum_{ij} \frac{1}{2} C V_{ij}^2,$$

results in

$$M = (\hbar/2e)^2 (2\pi/a)^2 C/2,$$

where  $C$  is the shunt capacitance of each junction.

<sup>19</sup>Vinay Ambegaokar and B. I. Halperin, *Phys. Rev. Lett.* **22**, 1364 (1969).

<sup>20</sup>M. Tinkham, *Introduction to Superconductivity* (McGraw-Hill, New York, 1975), p. 176 (reprinted by Krieger, Malabar, 1985).

<sup>21</sup>C. J. Lobb, *Physica B+C* **126**, 319 (1984).

<sup>22</sup>S. Teitel, *Physica B* **152**, 30 (1988).

<sup>23</sup>Thomas C. Halsey, *J. Phys. C* **18**, 2437 (1985).

<sup>24</sup>H. S. J. van der Zant, C. J. Muller, H. A. Rijken, B. J. van

Wees, and J. E. Mooij, *Physica B* **152**, 56 (1988).

<sup>25</sup>M. G. Forrester, H. J. Lee, M. Tinkham, and C. J. Lobb, *Phys. Rev. B* **37**, 5966 (1988).

<sup>26</sup>S. P. Benz, M. S. Rzchowski, M. Tinkham, and C. J. Lobb, *Phys. Rev. Lett.* **64**, 693 (1990).

<sup>27</sup>P. G. De Gennes, *Rev. Mod. Phys.* **36**, 225 (1964); G. Deutscher and P. G. De Gennes, in *Superconductivity*, edited by R. D. Parks (Marcel-Dekker, New York, 1969), Vol. II.

<sup>28</sup>In the theory of Ref. 19, the maximum in  $dV/dI$  approaches the critical current in the absence of fluctuations as the temperature is decreased. Even at finite temperature it is, in fact, a good approximation to the unfluctuated critical current [see C. M. Falco, W. H. Parker, S. E. Trullinger, and P. K. Hansma, *Phys. Rev. B* **10**, 1867 (1974)].

<sup>29</sup>Since  $E_J$  is the characteristic scale for vortex-vortex interactions as well as vortex-lattice interactions (Ref. 5), this technique eliminates the effects of sample to sample variations of the absolute coupling energy.

<sup>30</sup>K. K. Mon and S. Teitel, *Phys. Rev. Lett.* **62**, 673 (1989).

<sup>31</sup>S. Doniach and B. A. Huberman, *Phys. Rev. Lett.* **42**, 1169 (1979); B. A. Huberman and S. Doniach, in *Inhomogeneous Superconductors—1979*, (Berkeley Springs, WV), Proceedings of the Conference on Inhomogeneous Superconductors, AIP Conf. Proc. No. 58, edited by D. U. Gubser *et al.* (AIP, New York, 1979), p. 87.

<sup>32</sup>This assumes that the number of vortices in the sample is independent of temperature. We can confirm this by establishing that the applied field is always much greater than  $H_{c1}$ . Following the analysis of Huberman and Doniach (Ref. 31), and using LAT's result (Ref. 5) for  $\lambda_1$ ,  $H_{c1}$  is temperature independent and equal to  $(1/\pi R^2)\Phi_0 \ln(R/a)$ , where  $R$  is the sample radius. In our  $1000 \times 1000$  arrays, this is a field equivalent to only three vortices. Thus the vortex density in the sample is temperature independent, and not decreasing due to Meissner screening of the applied field.

<sup>33</sup>S. P. Benz, M. S. Rzchowski, M. Tinkham, C. J. Lobb, and G. O. Zimmerman, *Bull. Am. Phys. Soc.* **34**, 845 (1989).

<sup>34</sup>M. Tinkham, *Phys. Rev. Lett.* **61**, 1658 (1988).